Modulation of metal carbonyl stretching frequencies in the second coordination sphere through the internal Stark effect

Gemma L. Parker,[a] Ruben Van Lommel,[b,c] Nil Roig,[a,b] Mercedes Alonso*[b] and Adrian B. Chaplin*[a]

[a] Dr. G. L. Parker, N. Roig, Dr. A. B. Chaplin
Department of Chemistry, University of Warwick, Gibbet Hill Road, Coventry CV4 7AL (UK); E-mail: a.b.chaplin@warwick.ac.uk
[b] Dr. R. Van Lommel, N. Roig, Dr. M. Alonso
Eenheid Algemene Chemie (ALGC), Vrije Universiteit Brussel (VUB), 1050 Brussels Belgium; E-mail: mercedes.alonso.giner@vub.be
[c] Dr. R. Van Lommel
Molecular Design and Synthesis, Department of Chemistry, KU Leuven, 3001 Leuven, Belgium

Supporting information for this article is given via a link at the end of the document.

Abstract: Spectroscopic and computational examination of a homologous series of rhodium(I) pybox carbonyl complexes has revealed a correlation between the conformation of the flanking aryl-substituted oxazoline donors and the carbonyl stretching frequency. This relationship is also observed experimentally for octahedral rhodium(III) and ruthenium(II) variants and cannot be explained through the classical, Dewar–Chatt–Duncanson, interpretation of metal-carbonyl bonding. Instead, these findings are reconciled by local changes in the magnitude of the electric field that is projected along the metal-carbonyl vector: the internal Stark effect.

Introduction

Transition metal carbonyl complexes are seminal organometallic compounds with diverse fundamental and practical applications.[1] Coordination of carbon monoxide is classically characterised by a red-shifted stretching frequency ν(CO) and reconciled using the Dewar–Chatt–Duncanson bonding model, whereby population of the π*-orbitals through M→CO π-back donation weakens the CO bond (Fig. 1A).[2] This interpretation is the conceptual basis for the use of carbon monoxide as a spectroscopic reporter group and a ubiquitous feature of undergraduate chemistry textbooks.[3–6] The discovery of so called "non-classical" carbonyl complexes in the early 90s,[7] which exhibit shorter CO bond lengths and blue-shifted ν(CO) relative to free carbon monoxide, challenges this simplistic view and has renewed interest in the electronic structure of metal carbonyl complexes.[8,9]

The emerging theoretical consensus is that metal-carbonyl bonding involves superposition of metal-to-ligand charge transfer with electrostatic and orbital polarisation effects. The latter features can be viewed as the physical manifestation of the vibrational Stark effect,[9] the well-established phenomenon which describes how vibrational transition energies are perturbed by an electric field. For instance, an electric field applied along the C→O direction of free carbon monoxide is known to impose $\Delta\nu$(CO) > 0 due to the Stark effect (Fig. 1B).[10] Significantly, such electrostatic contributions are implicit in the coordination of carbon monoxide to metal cations and proposed, in extreme cases, to confer non-classical carbonyl complexes.

As part of our work exploring the organometallic chemistry of macrocyclic pincer complexes,[11] we observed that ν(CO) increases across the homologous series of rhodium(I) carbonyl complexes **1** – **3** (Fig. 1C). Supported by a detailed computational analysis, we herein demonstrate how these blue shifts can be attributed to persistent changes in the conformation of the flanking aryl-substituted oxazoline donors, which in turn give rise to an enhanced dipole moment along the metal-carbonyl vector. Whilst the effect of *external* electric fields on the spectroscopic properties of carbonyl complexes has previously been investigated, notably in the context of probing the structure of metalloenzyme active sites,[12] our experimental findings demonstrate the intrinsic role of *internal* electric fields in metal-carbonyl bonding.

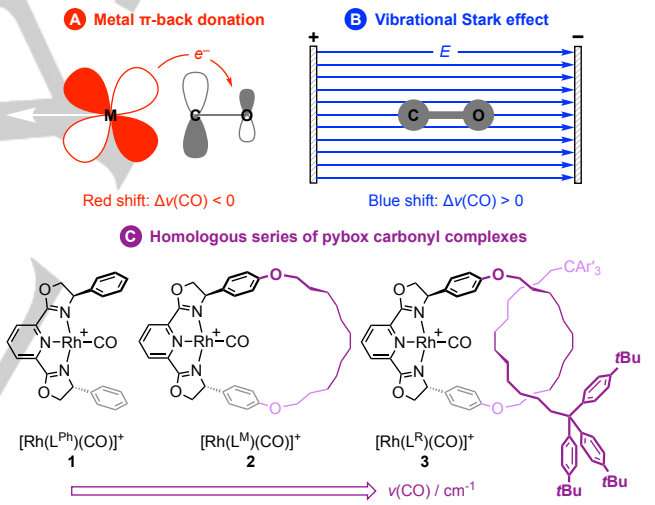

Figure 1. (A, B) Metal-based interactions with carbon monoxide and their effect on the carbonyl stretching frequency; (C) structures of the pybox carbonyl complexes studied, with $[BAr^F_4]^-$ counterions omitted for clarity (Ar^F = 3,5-$(CF_3)_2C_6H_3$).

Results and discussion

Complexes **1** – **3** are routine rhodium(I) carbonyl derivatives, but the synthetic complexity of the component pybox ligands varies considerably. Macrocyclic L^M is a known analogue of L^{Ph} and the new hydrocarbon threaded derivative L^R was prepared using a nickel-mediated $C(sp^3)$–$C(sp^3)$ homocoupling protocol developed by Leigh and co-workers for this macrocycle.[13] After adjusting the rotaxanation conditions to account for use of $Br(CH_2)_6CAr'_3$ (Ar′ = 4-*t*BuC_6H_4) as the half-axle, L^R was isolated in 18% yield following purification using reverse phase (C18) column chromatography to remove a doubly threaded [3]rotaxane that is formed in parallel in this instance (details provided in the supporting information). Capture of L^R was corroborated through perturbations to the ^{1}H

NMR resonances of the components and application of tandem mass spectrometry, with collision induced fragmentation of L^R into L^M observed within the ion trap of the spectrometer (Fig. S8/12). Acyclic **1** was readily prepared from L^{Ph} using a published two-step procedure that involves halide abstraction from the rhodium(I) chloride derivative and treatment with excess carbon monoxide.[3] This procedure was adapted for the more elaborate pybox-based ligands and the new rhodium(I) carbonyl derivatives **2** and **3** were ultimately isolated in good yield (76% and 59%, respectively, over two steps).[14]

The three carbonyl complexes adopt time averaged C_2 symmetry in CD_2Cl_2 solution at room temperature by ^1H and ^{13}C NMR spectroscopy. High frequency carbon resonances at δ 188 ppm also corroborate coordination of the carbonyl ligand and the associated $^{103}Rh–^{13}C$ coupling constants subtly decrease in the order **1** (76.5 Hz) > **2** (76.0 Hz) > **3** (75.4 Hz). More remarkably, when analysed in CH_2Cl_2 solution by IR spectroscopy, the value of ν(CO) measured for **3** (2030 cm^{-1}) was found to be appreciably blue-shifted relative to **2** (2022 cm^{-1}) and in turn **1** (2019 cm^{-1}). This trend is at odds with the classical, Dewar–Chatt–Duncanson, interpretation of metal-carbonyl bonding as it suggests significant changes in the donor characteristics of the pincer ligand. For instance, the Tolman electronic parameter of PPh_3 is 11 cm^{-1} higher than for PCy_3.[5]

DFT-based molecular dynamics simulations of **1** – **3** were selected to interrogate the origin of the spectroscopic differences *in silico*. Whilst considerably more computationally intense than traditional 'static' *ab initio* calculations, this approach enables the flexible nature of the macrocyclic ligands to be factored into the analysis through ensemble averaging of molecular properties over conformational isomers. Informed by previous work and benchmarking using **1**,[15] simulations were performed using the PBE functional and the DZVP-MOLOPT-GTH Gaussian plane-wave basis set with the cut-off and relative cut-off set at 250 Ry and 80 Ry, respectively.[16] Dispersion effects were captured through inclusion of Grimme's D3 dispersion correction.[17] Simulations ran within the NVT ensemble with the temperature set at 298 K and, to align with the timescale of an IR experiment, a time step of 0.5 fs was chosen. An equilibration phase of 5,000 steps preceded a production run of 20,000 steps. Wannier-based analysis on the final 10,000 steps enabled ensemble calculation of ν(CO) and the experimental trend is reproduced (**1**, 2016 cm^{-1}; **2**, 2018 cm^{-1}; **3**, 2026 cm^{-1}).[18]

The trajectories of **1** – **3** are characterised by considerable wobbling of the carbonyl ligand about the metal centre and across the coordination plane relative to conformational changes in the pybox core (Fig. 2). Static analysis of **1** at the B3PW91/6-31G(d,p) (SDD for Rh) level of theory confirmed that deviation of the py–Rh–CO unit from an ideal linear geometry is associated with a very flat potential energy surface and correlates this distortion with red-shifted ν(CO) ($\angle N_{py}$–Rh–C = 180→150°, ΔE < 4 kcal·mol^{-1}, $\Delta\nu$(CO) > –18 cm^{-1}).[19–21] Whilst differences in the rate of carbonyl precession about the metal can be discerned, **1** (13×10^{-3} fs^{-1}) ~ **2** (13×10^{-3} fs^{-1}) > **3** (9×10^{-3} fs^{-1}), invariant average values of $\angle N_{py}$–Rh–C suggest that the latter spectroscopic effect is not a significant factor for **1** – **3** (**1**, 172(4)°; **2**, 172(5)°; **3**, 172(4)°, **3**; Fig. 2). There are also no differences in the average Rh–C (**1**, 1.86(4), Å; **2**, 1.86(3) Å; **3**, 1.86(4) Å) and C≡O (**1**, 1.16(2) Å; **2**, 1.16(1) Å; **3**, 1.16(2) Å) bond lengths.

Significant disparities in the conformation of the oxazoline rings adopted in **1** – **3** were, however, identified from a wider geometric analysis of the simulations (Fig. 2). Most notably, more negative $\angle$O–C–C–C_{Ph} torsion angles were identified in **3** (–146(11)/–146(11)°) compared to **2** (–134(12)/–136(12)°) and in turn acyclic **1** (–124(16)/–123(16)°). Whilst it is was not initially clear to us how ν(CO) would be affected, these differences are supported experimentally in solution with **3** (9.6, 14.3 Hz) exhibiting more divergent oxazoline $^3J_{HH}$ coupling constants than **2** (10.1, 12.6 Hz) and moreover **1** (both ca. 9.8 Hz).[22] These net structural changes presumably reflect increasing conformational demands placed on the pybox ligand core, by incorporation of the dodecyldioxy strap in L^M and interpenetration of the hydrocarbon axle in L^R, and this interpretation is supported by qualitative inspection of the simulated structures.

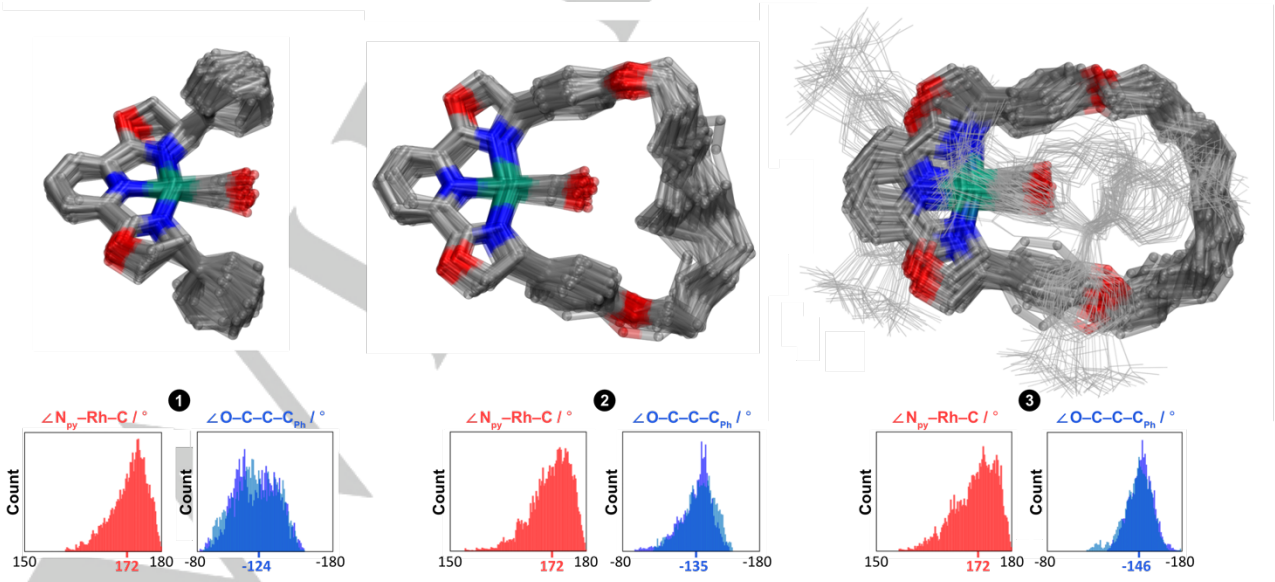

Figure 2. Summary of findings from the *ab initio* molecular dynamics simulations carried out at the PBE-D3/DZVP-MOLOPT-GTH level of theory. Overlayed simulated structures of **1** – **3** with H-atoms omitted and hydrocarbon thread in wireframe. Distributions of the $\angle N_{py}$–Rh–C and $\angle$O–C–C–C_{Ph} angles observed over the trajectories (average values in bold).

To determine how changes in oxazoline ring conformation could affect ν(CO) we returned to static DFT analysis of **1** at the B3PW91/6-31G(d,p) (SDD for Rh) level of theory. A relaxed potential energy scan was computed where the two ∠O–C–C–C_{Ph} torsion angles were synchronously varied between –121° and –161° in 2.5° steps (optimised value = –131°) and ν(CO) was determined at each point by Hessian analysis (Fig. 3A).[23] From this scan it can be concluded that these torsion angles correlate with a pincer-like movement of the phenyl substituents and scanning to more negative values of ∠O–C–C–C_{Ph} results in a substantial increase in ν(CO) (+8 cm^{-1}). The energetic penalties involved are small (4.5 kcal·mol^{-1}) but, through examination of the profile using the activation strain model (ASM) at the ZORA-PBE-D3/TZ2P level of theory,[24,25] independent of the how the carbonyl ligand interacts with the rhodium-pybox fragment (ΔE_{int} in Fig. 3B). Indeed, only a subtle decrease in the extent of π-back donation can be discerned along the scan by deconvolution of the orbital interactions for the rhodium-pybox/CO fragmentation using the extended transition state method for energy decomposition analysis, combined with the natural orbitals for chemical valence theory (ETS-NOCV, details provided in the supporting information).[26] The changes in energy along the scan are instead commensurate with the cost of distorting $[Rh(L^{Ph})]^+$ away from its equilibrium geometry (ΔE_{strain} in Fig. 3B). Drawing inspiration from theoretical studies examining the electronic structure of non-classical carbonyl complexes, the dipole moment (μ) of the rhodium-pybox fragment was assessed as a function of the ∠O–C–C–C_{Ph} torsion angles. The calculated dipole vector is coincident with the C_2 rotation axis, directed antiparallel to the carbon monoxide binding site (*i.e.* the associated electric field in **1** points in the C→O direction),[27] and increases 24% over the scan (Fig. 3C). Significantly, this increase in dipole moment directly parallels the calculated blue-shifts to the extent that the magnitude of μ and ν(CO) are linearly correlated with R^2 = 0.9996 (Fig. S66). On this basis, the increases in ν(CO) observed for **1** – **3** are attributed to local increases in the electric field projected along the metal-carbonyl vector that result from persistent changes in the conformation of the flanking aryl-substituted oxazoline donors (*cf.* $^3J_{HH}$ coupling constants). With respect to bonding models, our computational analysis confirms that these spectroscopic changes cannot be explained using the Dewar–Chatt–Duncanson model and that inclusion of the internal Stark effect is essential to fully describe the properties of the carbonyl complexes.

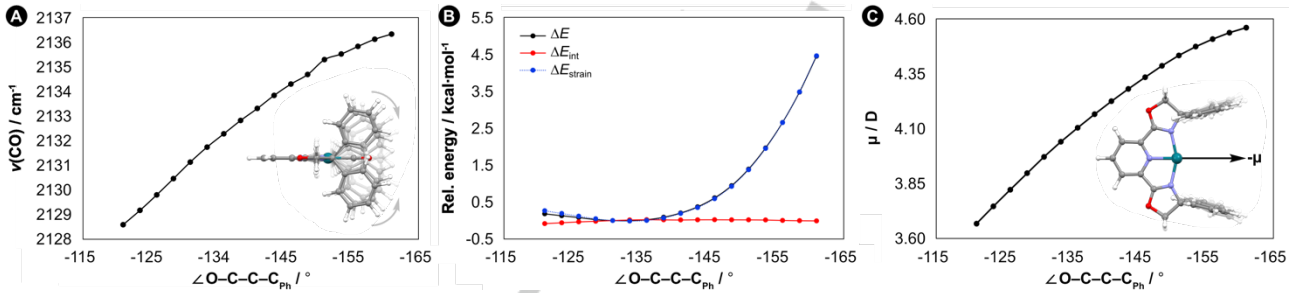

Figure 3. Relaxed potential energy scan for synchronous variation of the ∠O–C–C–C_{Ph} torsion angles in **1**: (A) change in carbonyl stretching frequency calculated at the B3PW91/6-31G(d,p) (SDD for Rh) level of theory, with insert illustrating the geometric changes; (B) ASM analysis of the $[Rh(L^{Ph})]^+$/CO fragmentation performed at the ZORA-PBE-D3/TZ2P level of theory; (C) calculated dipole moments of the $[Rh(L^{Ph})]^+$ fragment, with insert illustrating the geometric changes and inverse dipole direction (direction of associated electric field).

To substantiate our discovery experimentally, additional pybox carbonyl complexes where prepared, encompassing non-classical rhodium(III) $[Rh(pybox)Cl_2(CO)][BAr^F{}_4]$ (pybox = L^{Ph}, **4**;[3] L^M, **5**; L^R, **6**) and neutral ruthenium(II) $[Ru(pybox)Cl_2(CO)]$ (pybox = L^{Ph}, **7**; L^M, **8**; L^R, **9**) derivatives (5 new, details provided in the supporting information). As for the rhodium(I) homologues, these d^6-complexes adopt time averaged C_2 symmetry in CD_2Cl_2 solution on the ^{1}H NMR time scale and, when spectroscopically resolved, exhibit increasingly divergent oxazoline $^3J_{HH}$ coupling constants in the order L^{Ph} < L^M < L^R. Moreover, within experimental error, the values of ν(CO) measured for **4** – **9** in CH_2Cl_2 solution by IR spectroscopy reinforce the spectroscopic trend observed for **1** – **3** (Table 1). A small blue shift results from installation of the dodecyldioxy strap into the pybox ligand (L^M vs L^{Ph}), whilst an additional and larger blue shift occurs upon interpenetration of the hydrocarbon axle through the macrocycle (L^R vs L^M). The extent to which ν(CO) is affected is metal-fragment dependant, decreasing in the order $[Ru(pybox)Cl_2(CO)]$ > $[Rh(pybox)(CO)]^+$ > $[Rh(pybox)Cl_2(CO)]^+$, presumably reflecting the extent to which the C≡O bond is already polarised. Indeed, this suggestion is supported by the dipole moments calculated for the L^{Ph} complexes, which increase in the order $[Ru(L^{Ph})Cl_2]$ (3.37 D) < $[Rh(L^{Ph})]^+$ (3.97 D) < $[Rh(L^{Ph})Cl_2]^+$ (6.62 D).

Table 1. Carbonyl stretching frequencies of pybox complexes **1** – **9** (cm^{-1})[a]

	Acyclic L^{Ph}	Macrocyclic L^M	Rotaxane L^R
$[Rh^I(pybox)(CO)]^+$	2019[b]	2022	2030
$[Rh^{III}(pybox)(CO)]^+$	2151[b]	2150	2154
$[Ru^{II}(pybox)(CO)]$	1977	1980	1993

[a] Values confirmed by duplicate measurements, from which we estimate an error of ± 1 cm^{-1} under the conditions employed; [b] Data from reference 3.

Conclusion

Theoretical and experimental examination of a homologous series of rhodium(I) pybox carbonyl complexes has revealed a correlation between the conformation of the flanking aryl-substituted oxazoline donors and the carbonyl stretching frequency ν(CO). This relationship is also observed for octahedral rhodium(III) and ruthenium(II) variants and cannot be explained

through the classical, Dewar–Chatt–Duncanson, interpretation of metal-carbonyl bonding. Instead, these findings are reconciled by local changes in the magnitude of the electric field that is projected along the metal-carbonyl vector: the internal Stark effect. This interpretation is supported by a detailed computational analysis and emphasises why electrostatic and orbital polarisation effects should not be ignored in metal-carbonyl bonding models.

Experimental section

Full experimental and computational details are provided in the supporting information along with NMR, IR and ESI-MS spectra, and a conceptual overview of the ASM and ETS-NOCV methods (PDF format). Optimised geometries of **1**, **5** and **7** (XYZ format) and animations of the molecular dynamics simulations of **1**, **2** and **3** (MOV format) are also provided.

Deposition Numbers 2153016 (for **7**) and 2153017 (for **8**) contain the supplementary crystallographic data for this paper. These data are provided free of charge by the joint Cambridge Crystallographic Data Centre and Fachinformationszentrum Karlsruhe Access Structures service.

Acknowledgements

We thank the European Research Council (grant agreement 637313; G.L.P., A.B.C.), FWO Vlaanderen (1185221N, 12F4416N; R.V.L., M.A.), EUTOPIA alliance (N.R., M.A., A.B.C.), Vrije Universiteit Brussel (VUB, M.A.) and Royal Society (UF100592, UF150675; A.B.C.) for financial support. High-resolution mass-spectrometry data were collected using instruments purchased through support from Advantage West Midlands and the European Regional Development Fund. Crystallographic data were collected using an instrument that received funding from the ERC under the European Union's Horizon 2020 research and innovation programme (grant agreement No 637313). Tier2 computational resources and services were provided by the Shared ICT Services Centre funded by the VUB, the Flemish Supercomputer Center (VSC) and FWO. Tier1 computational resources and services were provided by the VSC, funded by the FWO and the Flemish Government-department EWI. R.V.L. thanks Dr. Ana V. Cunha for access to computational resources.

Keywords: carbonyl ligands • electrostatic interactions • bond theory • macrocyclic ligands • rotaxanes

[1] *Comprehensive Organometallic Chemistry IV* (Eds. G. Parkin, K. Meyer, D. O'Hare), Elsevier, **2022**.

[2] (a) D. M. P. Mingos, *J. Organomet. Chem.* **2001**, *635*, 1–8; (b) J. Chatt, L. A. Duncanson, *J. Chem. Soc.* **1953**, 2939–2947; (c) M. J. S. Dewar, *Bull. Soc. Chim. Fr.* **1951**, *18*, C79.

[3] G. L. Parker, S. Lau, B. Leforestier, A. B. Chaplin, *Eur. J. Inorg. Chem.* **2019**, 3791–3798.

[4] (a) L. Maser, C. Schneider, L. Vondung, L. Alig, R. Langer, *J. Am. Chem. Soc.* **2019**, *141*, 7596–7604; (b) J. J. Davidson, J. C. DeMott, C. Douvris, C. M. Fafard, N. Bhuvanesh, C.-H. Chen, D. E. Herbert, C.-I. Lee, B. J. McCulloch, B. M. Foxman, O. V. Ozerov, *Inorg. Chem.* **2015**, *54*, 2916–2935; (c) S. Wolf, H. Plenio, *J. Organomet. Chem.* **2009**, *694*, 1487–1492; (d) R. A. K. III, H. Clavier, S. Giudice, N. M. Scott, E. D. Stevens, J. Bordner, I. Samardjiev, C. D. Hoff, L. Cavallo, S. P. Nolan, *Organometallics* **2008**, *27*, 202–210; (e) A. R. Chianese, X. Li, M. C. Janzen, J. W. Faller, R. H. Crabtree, *Organometallics* **2003**, *22*, 1663–1667.

[5] C. A. Tolman, *Chem. Rev.*, 1977, **77**, 313–348.

[6] (a) R. H. Crabtree, *The Organometallic Chemistry of the Transition Metals*, 7th edition, Wiley, **2019**; (b) M. T. Weller, T. L. Overton, J. P. Rourke, F. A. Armstrong, *Inorganic Chemistry*, 7th edition, Oxford University Press, **2018**; (c) J. F. Hartwig, *Organotransition Metal Chemistry – From Bonding to Catalysis*, University Science Books, **2010**.

[7] (a) A. J. Lupinetti, S. H. Strauss, G. Frenking, *Prog. Inorg. Chem.* **2001**, *49*, 1–112; (b) P. K. Hurlburt, J. J. Rack, J. S. Luck, S. F. Dec, J. D. Webb, O. P. Anderson, S. H. Strauss, *J. Am. Chem. Soc.* **1994**, *116*, 10003–10014.

[8] Selected examples: (a) G. Frenking, I. Fernández, N. Holzmann, S. Pan, I. Krossing, M. Zhou, *JACS Au* **2021**, *1*, 623–645; J. Han, A. Grofe, J. Gao, *Inorg. Chem.* **2021**, *60*, 14060–14071; (b) S. C. C. van der Lubbe, P. Vermeeren, C. F. Guerra, F. M. Bickelhaupt, *Chem. Eur. J.* **2020**, *26*, 15690–15699; (c) G. Bistoni, S. Rampino, N. Scafuri, G. Ciancaleoni, D. Zuccaccia, L. Belpassi, F. Tarantelli, *Chem. Sci.* **2016**, *7*, 1174–1184; (d) M. Chen, Q. Zhang, M. Zhou, D. M. Andrada, G. Frenking, *Angew. Chem. Int. Ed.* **2015**, *127*, 126–130; (e) K. Nakashima, X. Zhang M. Xiang, Y. Lin, M. Lin, Y. Mo, *J. Theor. Comput. Chem.* **2008**, *7*, 639–654; (f) A. S. Goldman, K. Krogh-Jespersen, *J. Am. Chem. Soc.* **1996**, *118*, 12159–12166.

[9] (a) M. Loipersberger, Y. Mao, M. Head-Gordon, *J. Chem. Theory Comput.* **2020**, *16*, 1073–1089; (b) E. Rossomme, C. N. Lininger, A. T. Bell, T. Head-Gordon, M. Head-Gordon, *Phys. Chem. Chem. Phys.* **2020**, *22*, 781–798.

[10] S. Sowlati-Hashjin, C. F. Matta, *J. Chem. Phys.* **2013**, *139*, 144101.

[11] (a) T. M. Hood, A. B. Chaplin, *Dalton Trans.* **2021**, *50*, 2472–2482; (b) T. M. Hood, A. B. Chaplin, *Dalton Trans.* **2020**, *49*, 16649–16652; (c) B. Leforestier, M. R. Gyton, A. B. Chaplin, *Angew. Chem. Int. Ed.* **2020**, *59*, 23500–23504; (d) C. M. Storey, M. R. Gyton, R. E. Andrew, A. B. Chaplin, *Chem. Eur. J.* **2020**, *26*, 14715–14723; (e) B. Leforestier, M. R. Gyton, A. B. Chaplin, *Dalton Trans.* **2020**, *49*, 2087–2101; (f) T. M. Hood, M. R. Gyton, A. B. Chaplin, *Dalton Trans.* **2020**, *49*, 2077–2086; (g) M. R. Gyton, B. Leforestier, A. B. Chaplin, *Organometallics* **2018**, *37*, 3963–3971; (h) C. M. Storey, M. R. Gyton, R. E. Andrew, A. B. Chaplin, *Angew. Chem. Int. Ed.* **2018**, *57*, 12003–12006; (i) S. L. Apps, R. E. Alflatt, B. Leforestier, C. M. Storey, A. B. Chaplin, *Polyhedron* **2018**, *143*, 57–61; (j) R. E. Andrew, C. M. Storey, A. B. Chaplin, *Dalton Trans.* **2016**, *45*, 8937–8944; (k) R. E. Andrew, D. W. Ferdani, C. A. Ohlin, A. B. Chaplin, *Organometallics* **2015**, *34*, 913–917; (l) R. E. Andrew, A. B. Chaplin, *Inorg. Chem.* **2015**, *54*, 312–322; (m) R. E. Andrew, A. B. Chaplin, *Dalton. Trans.* **2014**, *43*, 1413–1423.

[12] (a) S. Bhunia, A. Ghatak, A. Dey, *Chem. Rev.* **2022**, *122*, 12370–12426; (b) S. D. Fried, S. G. Boxer, *Acc. Chem. Res.* **2015**, *48*, 998–1006; (c) S. D. Dalosto, J. M. Vanderkooi, K. A. Sharp, *J. Phys. Chem. B* **2004**, *108*, 6450–6457; (d) E. S. Park, S. S. Andrews, R. B. Hu, S. G. Boxer, *J. Phys. Chem. B.* **1999**, *103*, 9813–9817; (e) T. Li, M. L. Quillin, G. N. Phillips, J. S. Olson, *Biochemistry* **1994**, *33*, 1433–1446.

[13] S. M. Goldup, D. A. Leigh, R. T. McBurney, P. R. McGonigal, A. Plant, *Chem. Sci.* **2010**, *1*, 383–386.

[14] Rotaxane complex **3** reversibly binds a second equivalent of carbon monoxide under the experimental conditions employed in the synthesis (Fig. S44/45). Persistent deviation of the carbonyl ligand from an ideal linear coordination geometry is, however, not supported by variable temperature analysis of isolated **3** by ^{1}H NMR spectroscopy, where sharp oxazoline signals and time averaged C_2 symmetry were observed down to 185 K in THF-d_8 (600 MHz; Fig. S48/49).

[15] (a) C. S. Praveen, A. Comas-Vives, C. Copéret, J. VandeVondele, *Organometallics*, **2017**, *36*, 4908–4919; (b) N. Govindarajan, A. Tiwari, B. Ensing, E. J. Meijer, *Inorg. Chem.* **2018**, *57*, 13063–13066.

[16] J. VandeVondele, J. Hutter, *J. Chem. Phys.* **2007**, *127*, 114105.

[17] S. Grimme, J. Antony, S. Ehrlich, H. Krieg, *J. Chem. Phys.* **2010**, *132*, 154104.

[18] M. Brehm, M. Thomas, S. Gehrke, B. Kirchner, *J. Chem. Phys.* **2020**, *152*, 164105.

[19] Previous work has shown that this functional can accurately describe the geometry of rhodium pincer complexes with structures similar to **1**. For recent examples see: (a) C. M. Storey, A. Kalpokas, M. R. Gyton, T. Krämer, A. B. Chaplin, *Chem. Sci.* **2020**, *11*, 2051–2057; (b) N. Hara, T. Saito, K. Semba, N. Kuriakose, H. Zheng, S. Sakaki, Y. Nakao, *J. Am. Chem. Soc.* **2018**, *140*, 7070–7073.

[20] (a) A. D. Becke, *J. Chem. Phys.* **1993**, *98*, 5648–5652; (b) A. W. Ehlers, M. Böhme, S. Dapprich, A. Gobbi, A. Höllwarth, V. Jonas, K. F. Köhler, R. Stegmann, A. Veldkamp, G. Frenking, *Chem. Phys. Lett.* **1993**, *208*, 111–114; (c) D. Andrae, U. Häußermann, M. Dolg, H. Stoll, H. Preuß, *Theor. Chem. Act.* **1990**, *77*, 123–141; (d) A. D. Becke, *Phys. Rev. A* **1988**, *38*, 3098–3100; (e) R. Ditchfield, W. J. Hehre, J. A. Pople, *J. Chem. Phys.* **1971**, *54*, 724–728.

[21] Subtle changes in metal coordination geometry can significantly affect the spectroscopic characteristics of metal carbonyl complexes: S. C. Meier, D. Himmel, I. Krossing, *Chem. Eur. J.* **2018**, *24*, 19348–19360.

[22] Calculated oxazoline $^{3}J_{HH}$ coupling constants for **1** as a function of the ∠O–C–C–C_{Ph} torsion angles are provided as part of the electronic supporting information for comparison (Fig. S68).

[23] Physically meaningful changes in calculated *ν*(CO) are supported by comparable changes in the CO bond delocalisation index (Fig. S65).

[24] (a) P. Vermeeren, S. C. C. van der Lubbe, C. Fonseca Guerra, F. M. Bickelhaupt, T. A. Hamlin, *Nat. Prot.* **2020**, *15*, 649–667; (b) F. M. Bickelhaupt, K. N. Houk, *Angew. Chem. Int. Ed.* **2017**, *56*, 10070–10086; (c) G. te Velde, F. M. Bickelhaupt, E. J. Baerends, C. Fonseca Guerra, S. J. A. van Gisbergen, J. G. Snijders, T. Ziegler, *J. Comput. Chem.* **2001**, *22*, 931–967.

[25] (a) E. Van Lenthe, E. J. Baerends, *J. Comput. Chem.* **2003**, *24*, 1142–1156; (b) J. P. Perdew, K. Burke, M. Ernzerhof, *Phys. Rev. Lett.* **1996**, *77*, 3865–3868; (c) E. van Lenthe, E. J. Baerends, J. G. Snijders, *J. Chem. Phys.* **1994**, *101*, 9783–9792; (d) E. v. Lenthe, E. J. Baerends, J. G. Snijders, *J. Chem. Phys.* **1993**, *99*, 4597–4610.

[26] (a) L. Zhao, M. von Hopffgarten, D. M. Andrada, G. Frenking, *WIREs Comput. Mol. Sci.* **2018**, *8*, e1345; (b) M. P. Mitoraj, A. Michalak, T. Ziegler, *J. Chem. Theor. Comput.* **2009**, *5*, 962–975.

[27] The IUPAC convention for the direction of the dipole moment is from negative to positive charge. https://doi.org/10.1351/goldbook.E01929 (accessed 14/07/2022).

Entry for the Table of Contents

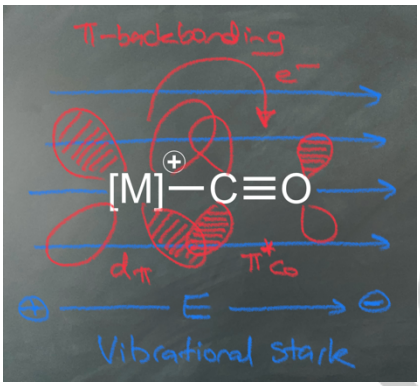

Carbonyl stretching frequencies of late transition metal pybox complexes demonstrate the intrinsic role of *internal* electric fields in metal-carbonyl bonding.

Institute and/or researcher Twitter usernames: **@ALGC_VUB**, **@chaplinlab**